

# Numerical simulations of aeroelastic instabilities in a turbine-blade cascade by a modified Van der Pol model at running excitation

L. Pešek<sup>a,\*</sup>, P. Šnábl<sup>a</sup>, C. S. Prasad<sup>a</sup>, Y. Delanney<sup>a</sup>

<sup>a</sup>*Institute of Thermomechanics, Czech Academy of Sciences, Dolejškova 5, 182 00 Prague, Czech Republic*

Received 5 October 2022; accepted 14 March 2023

---

## Abstract

The onset and spread of flutter in a turbine blade cascade are numerically studied. Due to the application of the reduced-cascade model consisting of simple elements (springs, rigid bodies, linear dampers) and aeroelastic forces introduced by the analytical Van der Pol model, it is useful to study the dangerous states of vibration of such complicated turbine parts. This study examines aeroelastic instabilities of a 10-blade cascade at running excitation that arise due to wakes flowing from the stator blades to the rotating blades. Unlike our previous work, it brings a new definition of the Van der Pol model of self-excitation that is controlled by relative inter-blade motion of neighbouring blades.

© 2023 University of West Bohemia.

*Keywords:* flutter, blade cascade, self-excitation, Van der Pol

---

## 1. Introduction

Along with a rotary test rig for evaluation of structural dynamics of bladed wheels, controlled flutter experiments have been performed on a linear cascade model in the subsonic wind tunnel at the Institute of Thermomechanics of the Czech Academy of Sciences. The aim of these experiments is to evaluate the stability limits of the cascade using deformation waves, flow velocity changes or blade force impulses. The onset and spread of flutter in the cascade are observed, as well. The linear cascade model consists of five NACA 010 blades. Each blade can be separately excited by an electromagnetic torque excitation mechanism. All blades are instrumented to measure the aerodynamic moments, which can be used to calculate the aerodynamic work. More details about the linear blade cascade experimental setup can be found in [3, 11].

To predict dynamic behavior of the blade cascade, we have also used a simplified theoretical model of the aeroelastic instability for turbine blade cascades [2, 4, 7]. Due to the application of the reduced cascade model consisting of simple elements (springs, rigid bodies, linear dampers) and aeroelastic forces introduced by analytical Van der Pol model, a study of the dangerous states of vibration of such complex turbine parts [8, 13] can be facilitated.

This paper follows the previous work [4] and examines aeroelastic instabilities of a 10-blade cascade at running excitation that arises due to the wakes flowing from the stator blades to the rotating blades, which causes forced excitation in a narrow frequency range. This work is aimed at better understanding the complexity of the dynamics of turbine-bladed wheels at the flutter self-excitation state.

---

\*Corresponding author. Tel.: +420 266 053 083, e-mail: pesek@it.cas.cz.  
<https://doi.org/10.24132/acm.2023.792>

Unlike the previous study, the present work provides a new definition of the Van der Pol model of self-excitation. The former one was controlled by the total vibrational motion of the blade. For this case, however, we consider a modified form of the Van der Pol model. Instead of the total motion of individual blade profile, the model is controlled by relative inter-blade motion of neighbouring blades. According to the flutter theory of blade cascades, both movements are important for flutter origin [1,9,10,12]. The first form was linked to the classical single aerofoil instability, and the modified form is linked to instability of blade cascades caused by the excitation of travelling waves [5,6].

## 2. Motion equations of turbine blade cascade with self-excitation

The studied cascade consists of single-blade subsystems, where each blade can undergo pitch torsional and vertical transverse motions, as shown in Fig. 1. All blades are considered as elastic bodies. However, since we are examining their dynamic properties in a narrow frequency band, e.g., around the first eigenfrequency of torsion or transverse motion, it is possible to model each blade as a two degree of freedom (DOF) system.

The centre of mass  $m$  of the 2 DOF blade profile is represented by point  $T$ , see Fig. 1, and the moment of inertia is denoted by  $I$ . The flexural axis of this profile is represented by  $O_1$  and the transitional stiffness in the vertical direction  $y$  is  $k$ . The pitch spring stiffness around this flexural axis is  $k_t$  and it is connected in parallel with a damping element having the torsional damping coefficient  $b_t$ . Parallel to the elastic force, there is a viscous damping force with the coefficient  $b$ . The vertical aerodynamic force  $F$  acting on the blade in the direction  $y$  is shifted by the distance  $e_2$  to the point  $O_2$ . Additionally, there is an aeroelastic moment  $M_e = F(e_1 + e_2)$  acting around the flexural axis  $O_1$  and oriented by the pitch angle  $\alpha$ .

The dynamic model of the blade cascade is schematically shown in Fig. 2. The blade inter-connections  $g_i$  are defined by the stiffness  $k_1$  and by the viscous damping  $b_1$ . These visco-elastic connections between neighbouring blades can express the dynamic properties of connections in turbine disk, blade shroud or damping wires.

The aerodynamic forces  $F_{e,i}$  act on the blades at points  $O_2$  at the distance of  $e_2 = 0.005$  m from the elastic axes  $O_1$ . There are two types of these aerodynamic forces:

1. The velocity of steam flowing from the stator cascade has a periodic profile due to the distortion of stator blades and the wakes of flow from the stator blades produce forced vibration of the rotating blades. Different numbers of blades of rotor and stator wheels cause the phase delays of excitation forces produced by these wakes.
2. The flowing steam through the rotating blade cascade produces, besides the aforemen-

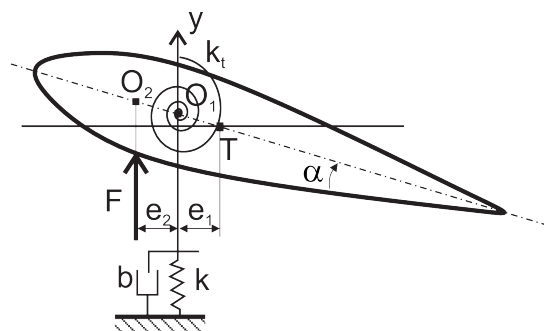


Fig. 1. Dynamic model of blade profile

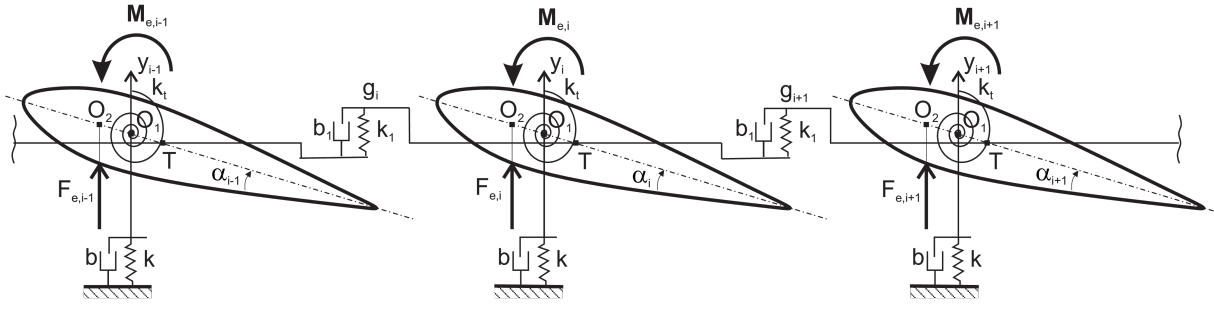


Fig. 2. Diagram of blade cascade section

tioned periodic forced vibration, vertical and torsional aeroelastic self-exciting forces  $F_{e,i}$  and  $M_{e,i}$ , respectively (Fig. 2).

Both of the excitation sources mutually interact and the running waves of forced vibration initiate the flutter running waves. Steam flowing through the rotating blade cascade can cause a decrease of damping and aeroelastic flutter instability. Since an exact description of this aeroelastic phenomenon is very complicated, we proposed the Van der Pol model [5], which can describe two aerodynamic effects: the first one acting on individual blades controlled by only one blade's motion, and the second one related to interacting blades and controlled by relative motions of neighbouring blades. The first form of the Van der Pol model is described by the equation

$$G_i = -\mu_0 \left[ 1 - \left( \frac{y_i}{r_y} \right)^2 \right] \dot{y}_i \quad (1)$$

and the other one by the modified equation

$$F_{eV,i} = -\mu_1 \left[ 1 - \left( \frac{y_i - y_{i-1}}{r_y} \right)^2 \right] (\dot{y}_i - \dot{y}_{i-1}) + \mu_1 \left[ 1 - \left( \frac{y_{i+1} - y_i}{r_y} \right)^2 \right] (\dot{y}_{i+1} - \dot{y}_i), \quad (2)$$

where  $G_i$ ,  $F_{eV,i}$  are the aerodynamic forces,  $y_i$ ,  $\dot{y}_i$  are vertical displacements and blade velocity,  $r_y$  is the blade displacement where the aerodynamic force changes its sign, and  $\mu_0$ ,  $\mu_1$  denote the intensity coefficients of the Van der Pol models (1)–(2). Equation (2) describes the force couplings of the  $i$ -th blade with the motions of both neighbouring blades.

Analogous to (2), we can introduce also the Van der Pol moment arising from pitch motion  $\alpha$  of the profile as

$$M_{e,i} = -\mu_2 \left[ 1 - \left( \frac{\alpha_i - \alpha_{i-1}}{r_\alpha} \right)^2 \right] (\dot{\alpha}_i - \dot{\alpha}_{i-1}) + \mu_2 \left[ 1 - \left( \frac{\alpha_{i+1} - \alpha_i}{r_\alpha} \right)^2 \right] (\dot{\alpha}_{i+1} - \dot{\alpha}_i). \quad (3)$$

The blades in the rotating bladed row are excited by external periodic forces arising from the rotation of the bladed wheel with  $l_r$  blades exposed to the spatially periodical steam flow from the stator blade cascade with another number  $l_s$  of blades ( $l_r \neq l_s$ ). The periodic force exciting the  $i$ -th blade by the wakes of steam flow can be simplified to the first harmonic component  $F_{0i} = \cos[\omega t - (i - 1)\Delta\varphi]$ , where the excitation frequency  $\omega$  depends on the wheel rotation,  $\omega_r = \omega/l_r$ . The phase delay  $\Delta\varphi$  of harmonic excitation forces depends on the ratio  $l_s/l_r$  of rotor and stator blade numbers according to the following relation:

$$\Delta\varphi = 2\pi \left( 1 - \frac{l_s}{l_r} \right). \quad (4)$$

The phase shift  $\Delta\varphi$  is non-zero due to the different numbers of blades of stationary and rotating disks ( $l_r \neq l_s$ ). This causes a running wave in the blade cascade: (i) forward wave if  $l_s/l_r < 1$ , then  $\Delta\varphi > 0$ , and (ii) backward wave if  $l_s/l_r > 1$ , then  $\Delta\varphi < 0$ . The period of blade excitation  $T_w$  is given by the time difference of passing from one stator blade to the adjacent one, that is  $T_w = 2\pi/(l_s\omega_r)$ , where  $\omega_r$  is the angular revolution frequency.

When the periodic excitation forces and the modified type of the Van der Pol forces (2)–(3) are applied, differential equations of the blade cascade (Fig. 2) can be derived by the d'Alembert principle:

$$m\ddot{y}_i + \frac{k_t m e_1}{I} \alpha_i + \left(k + \frac{k m e_1^2}{I}\right) y_i + b\dot{y}_i + F_{eV,i} + g_i - g_{i+1} = F_{0i} \cos[\omega t - (i-1)\Delta\varphi], \quad (5)$$

$$I\ddot{\alpha}_i + k_t \alpha_i + b_t \dot{\alpha}_i - (e_1 + e_2) F_{eV,i} + M_{e,i} + k e_1 y_i = (e_1 + e_2) F_{0i} \cos[\omega t - (i-1)\Delta\varphi],$$

$i = 1, \dots, 10$ , where  $g_i = k_1(y_i - y_{i-1}) + b_1(\dot{y}_i - \dot{y}_{i-1})$  are the viscoelastic connections between blades. Conditions  $g_{11} = g_1$ ,  $F_{eV,11} = F_{eV,1}$ ,  $M_{e,11} = M_{e,1}$  preserve the circular periodicity of the system.

As seen in (5), the negative self-exciting forces  $F_{eV,i}$  are compensated by positive structural damping with coefficient  $b$ . Self-excited oscillations can arise if  $\mu > b$ , but it needs an initial impulse to trigger it. Since our goal was to simulate instabilities in the experimental cascade for relative blade motions with predominant torsional pitch, only the Van der Pol moment according to (3) was considered, and therefore the remaining intensity coefficients  $\mu_0, \mu_1$  were set to zero.

The 10-blade cascade case is considered in the numerical simulations in the following sections. The solution of (5) was ascertained by the Runge-Kutta method of the fourth order.

### 3. Estimation of the intensity coefficient of the Van der Pol model

The numerical simulations based on (5) can be used to estimate the intensity coefficient of the designed Van der Pol model by comparison with the experimental results of aerodynamic (AD) damping. For the demonstration, we chose the AD damping S-curve for one experimental configuration [1]: linear 5-blade cascade at fluid velocity  $30 \text{ m s}^{-1}$ , stagger angle  $30^\circ$ , angle of attack  $-10^\circ$ , at torsional travelling vibration mode – frequency  $40 \text{ Hz}$ , vibration amplitude  $2^\circ$ , phase angle from interval  $(-\pi, \pi)$ .

The input parameters used in our simulation were chosen as:  $m = 0.18 \text{ kg}$ ,  $b = 2 \text{ kg s}^{-1}$ ,  $k = 50\,000 \text{ kg s}^{-2}$ ,  $I = 0.000\,025 \text{ kg m}^2$ ,  $k_t = 1 \text{ kg m}^2 \text{ s}^{-2}$ ,  $e_1 = e_2 = 0.005 \text{ m}$ ,  $b_t = 0.000\,05 \text{ kg m}^2 \text{ s}^{-2} \text{ rad}^{-1}$ . These parameters yield the eigenfrequencies  $\Omega_1 = 182.24 \text{ rad s}^{-1}$  and  $\Omega_2 = 578.42 \text{ rad s}^{-1}$  and the damping ratios  $0.5\%$  and  $1.05\%$  of a single-blade subsystem for torsional and vertical vibrations, respectively. To match these eigenfrequencies to experimental ones, the parameters of the mass  $m$  and the moment of inertia  $I$  of the profile, the stiffnesses  $k, k_t$  and the damping coefficients  $b, b_t$  of the vertical and torsional blade suspensions were identified by using corresponding experimental eigenfrequencies and damping ratios.

To evaluate the AD damping by the numerical simulations of travelling waves in the cascade, we needed to suppress all transients of vibration; hence, an increase of the structural damping was necessary. With higher damping ( $50\%$  for torsional and  $22\%$  for vertical vibrations) and longer integration times, we could preserve the harmonic motion of the blades with a prescribed phase shift, which is inevitable for the evaluation of AD damping. Time characteristics of amplitudes of vertical and angular displacements and aerodynamic moment of the first blade at excitation frequency  $40 \text{ Hz}$  and  $\Delta\varphi = -2\pi/5$  are shown in Fig. 3.

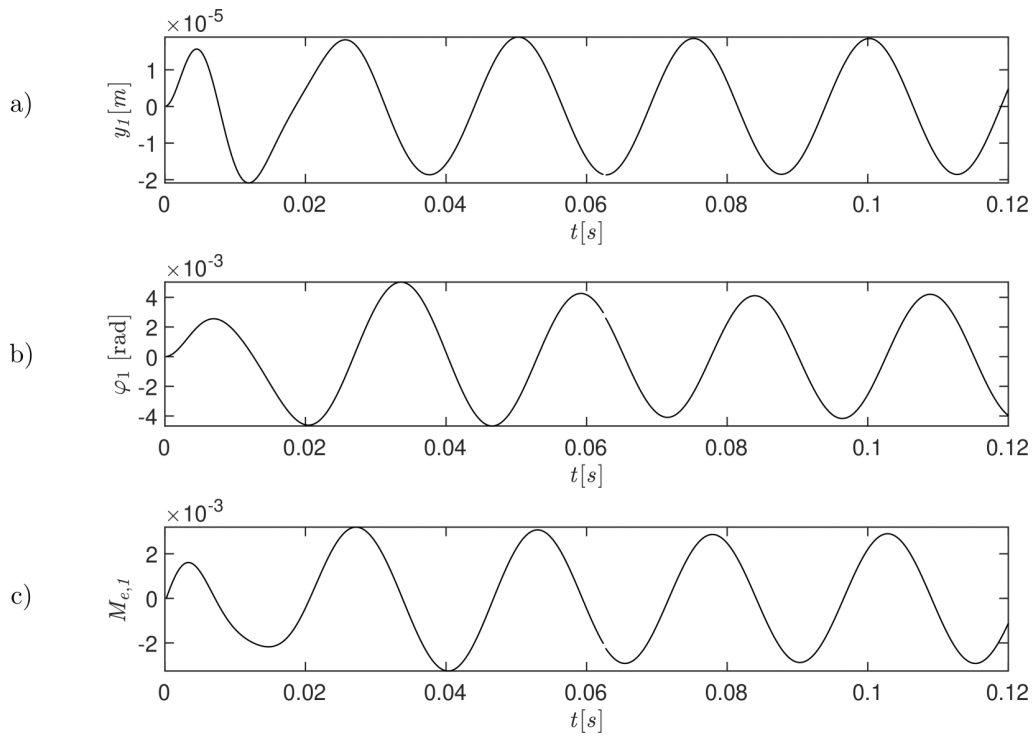


Fig. 3. Time characteristics of the first blade at the excitation frequency 40 Hz and  $\Delta\varphi = -2\pi/5$ : amplitudes of (a) vertical and (b) angle displacements, (c) aerodynamic moment

The comparison between experimental and calculated AD damping with respect to the phase angle  $\Delta\varphi$  can be seen in Fig. 4. The values of calculated AD damping are plotted for three values of intensity coefficient  $\mu_2$  (0.001, 0.001 5, and 0.002) with a step of  $\pi/5$  since it corresponds to a step increase in the number of nodal diameter (ND) of the travelling mode. The phase angle and the number of ND are linked by relation  $\Delta\varphi = 2\pi\text{ND}/l_r$ . It can be seen that the AD damping waveform calculated for the Van der Pol model has amplitude-shifted cosine waveforms with respect to the sinusoidal waveform of the experimental data. Therefore, the Van der Pol model always leads to self-excited vibrations (negative AD damping) for both forward (+ phase angles) and backward (– phase angles) travelling waves. Consequently, the Van der Pol model cannot be tuned by the coefficient  $\mu_2$  to the experimental S-curve in the whole interval of phase angles. But since the flutter is a strictly resonant phenomenon linked to a certain number of ND, we can tune the Van der Pol model to this ND mode. For example, for 2 ND case we can estimate  $\mu_2$  between 0.001 5 and 0.002 since the experimental one lies between their waveforms (Fig. 4).

#### 4. Numerical simulations of flutter onset by increasing the intensity coefficient

To study flutter onset in the cascade due to gradually increasing flow velocity that increases flow instability, we dealt with numerical simulations of flutter, gradually increasing the intensity coefficient.

We considered its linear growth over time given by the coefficient  $c_\mu$ . To include this dependency in the simulation, we extended the system of differential equations (5) by an equation of the first order  $\dot{\mu}_2 = c_\mu$  with the initial condition  $\mu_2(0) = 5 \times 10^{-4} \text{ kg s}^{-1}$  and the constant  $r_\alpha = 0.1745 \text{ rad}$ . We chose two cases of inter-blade viscous-elastic Kelvin-Voigt

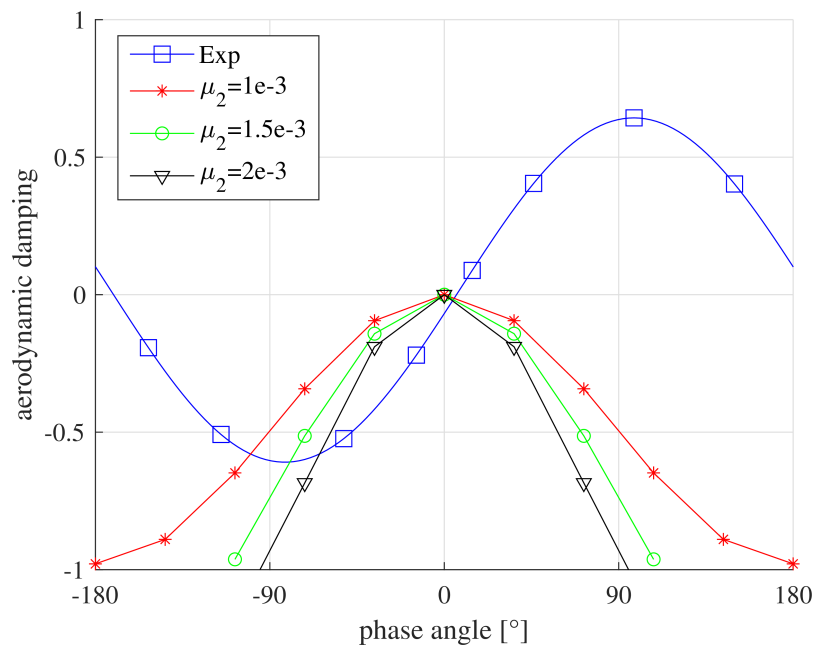


Fig. 4. AD damping waveforms: experimental S-curve for velocity  $0 \text{ m s}^{-1}$ , incident angle  $-10^\circ$ , excitation frequency  $40 \text{ Hz}$ , vibration amplitude  $2^\circ$ , stagger angle  $30^\circ$  (curve  $\square$ ) and calculated sets for parameter  $\mu_2 = 0.001$  (curve  $*$ ),  $0.0015$  (curve  $\circ$ ),  $0.002$  (curve  $\nabla$ )

connections: A) without connections ( $k_1 = 0 \text{ kg s}^{-2}$ ,  $b_1 = 0 \text{ kg s}^{-1}$ ), B) with connections ( $k_1 = 10\,000 \text{ kg s}^{-2}$ ,  $b_1 = 0.2 \text{ kg s}^{-1}$ ). The first case corresponds to cascades with no linkages between them, e.g., via disk, and only damping connections are via modified Van der Pol model of flow aeroelastic forces. In the second case, both structural and aeroelastic connections are considered. Response curves are computed in the following examples for backward running force excitation when  $\Delta\varphi = -2\pi/5$  at the nozzle excitation frequency  $\omega = 62.8 \text{ rad s}^{-1}$ . It corresponds to 12 stator blades and to the revolution frequency  $1.25 \text{ Hz}$ . The structural profiles parameters mentioned above and amplitude of external wake force  $F_0 = 0.01 \text{ N}$  were applied, as well. The value of the excitation force was numerically identified so that the loss of stability does not occur immediately after starting the calculation from initial conditions due to the experimentally-identified damping ratios of the blades' visco-elastic suspension.

#### 4.1. Study case A – Cascade without inter-blade structural connections

The time characteristics of the first blade displacements and its aerodynamic moment (Fig. 5) show that flutter arises at time ca.  $1.2 \text{ s}$  when the intensity coefficient achieves a value ca.  $0.001$ . Due to arising self-excited vibrations at the first torsional eigenfrequency, the dominant vibration is observed at torsional mode, but it causes also increasing vertical displacements. Even after stabilization of vibrations at time  $1.5 \text{ s}$ , the amplitude of vibrations is not constant, and the course of vibration is non-stationary. The motions of other blades have similar time displacement characteristics, but they are phase-shifted. The distribution of amplitudes of blades in the cascade can be seen on the vibration shapes in Figs. 11, 12, 19, 20.

From the phase diagrams in Figs. 6–7, it can be seen that the angular torsional vibration (b) of the first blade had an almost periodical character. To show the evolution of the phase diagram, the colours change with increasing time of calculation intervals – red (0, 1) s, yellow (1, 1.5) s, violet (1.5, 2) s, dark blue (2, 3) s, light blue (3, 4) s. The highly non-linear character can be

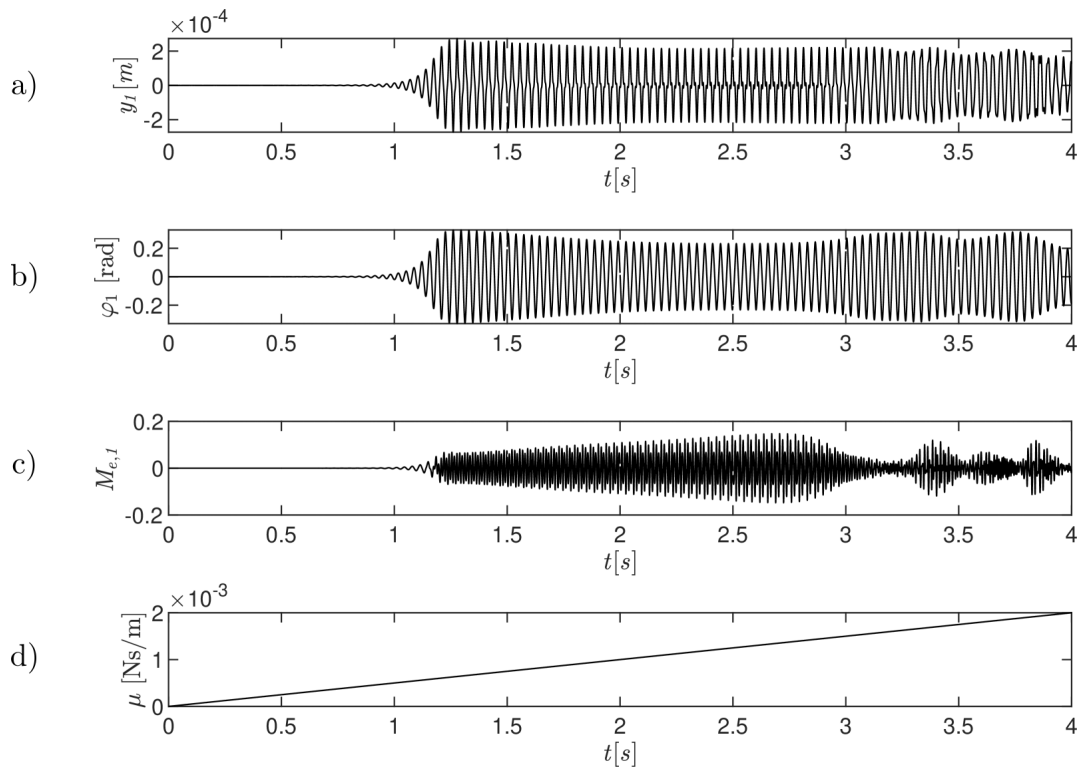


Fig. 5. Time characteristics of amplitudes of (a) vertical and (b) angular displacements of the first blade, of (c) aerodynamic moment of the first blade and of (d) intensity coefficient at excitation frequency 10 Hz and  $\Delta\varphi = -2\pi/5$

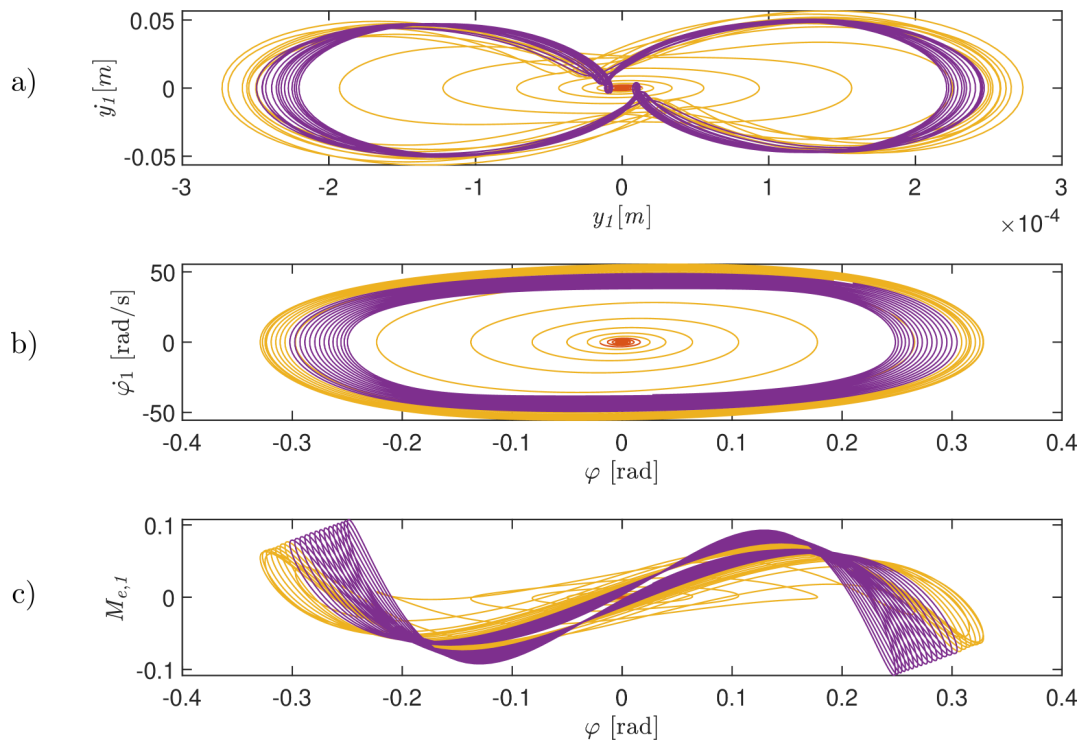


Fig. 6. Phase diagrams in interval (0, 2) s: (a) vertical and (b) angle responses of the first blade, (c) hysteresis loops of aerodynamic moment versus angular displacement of the first blade at excitation frequency 10 Hz and  $\Delta\varphi = -2\pi/5$

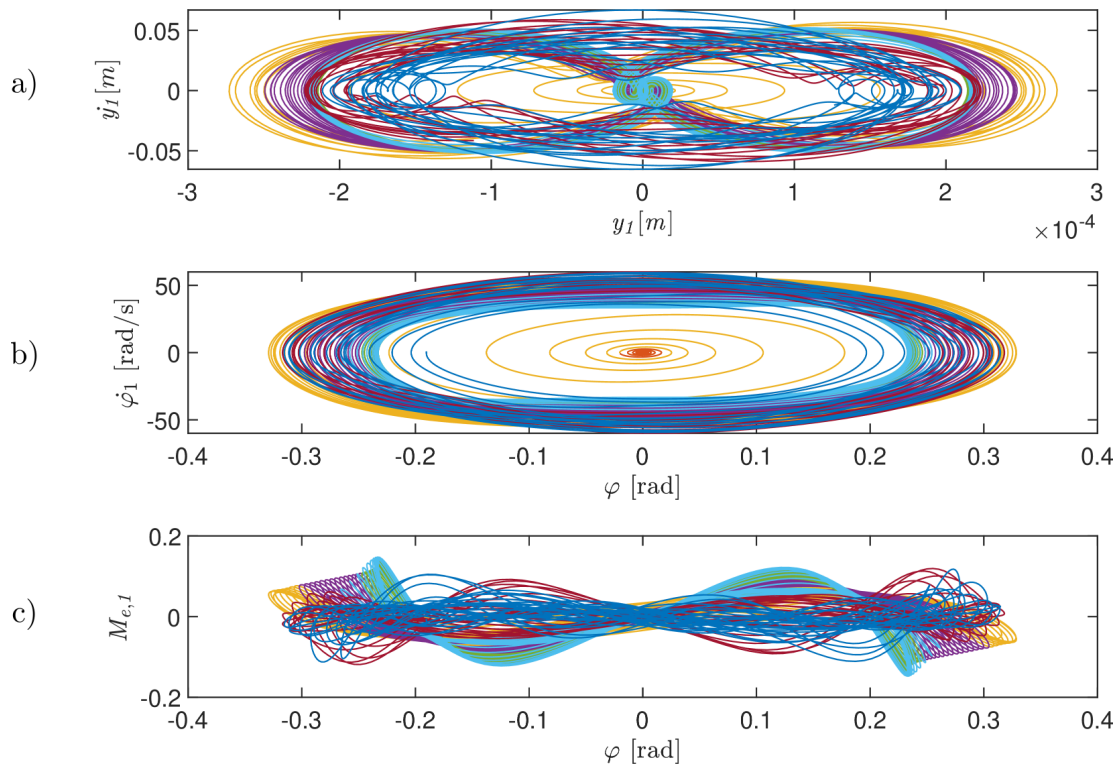


Fig. 7. Phase diagrams in interval (0, 4) s: (a) vertical and (b) angular responses of the first blade, (c) hysteresis loops of aerodynamic moment versus angular displacement of the first blade at excitation frequency 10 Hz and  $\Delta\varphi = -2\pi/5$

seen on the vertical displacement diagram where the motion has a quasi-harmonic character but is not fully stable. The same is valid also for hysteresis curves of the aerodynamic moment. The loops and their time evolution show that during one period of vibration, there are both excitation and damping effects of the Van der Pol model.

The motions of other blades have similar time displacement and phase diagrams, but they are phase-shifted in time. The vertical and distortion displacements of all 10 blades in the interval (3.5,3.7) s are plotted in Figs. 8 and 9, respectively, and the wheel amplitude distribution can be seen on the vibration mode for three selected times (1 s, 2 s, 4 s) in Fig. 11 and on the vibration mode of the wheel at time 3.999 8 s (Fig. 12), as well.

Although the backward-running force mode was applied to the cascade (Fig. 10), due to flutter self-excitation leading to forced resonant vibration of the cascade, the travelling character of vibration modes was weak in developed states of flutter, as seen in Figs. 8–9.

In Fig. 11, we can see the mode of vibration across the cascade at certain times: a) at the onset of flutter, b) at the flutter state. It is clear that until the onset of the flutter, the mode of vibration has an eigenmode shape with 2 ND and this mode is travelling. However, in the state of flutter, the vibration mode becomes more complex as the number of ND increases. Both of these modes are still travelling. However, for longer times (above 3.7 s) when the flutter is more developed, a mode of 4 ND prevails at the vibration and this travelling mode becomes standing (Fig. 12).

The maximal amplitude diagram in Fig. 13 shows multiple maxima during one excitation period of 0.1 s. At the onset of self-excited oscillation (1.3 s), this phenomenon is caused by shorter vibration period in one excitation period due to the resonant torsional vibration with

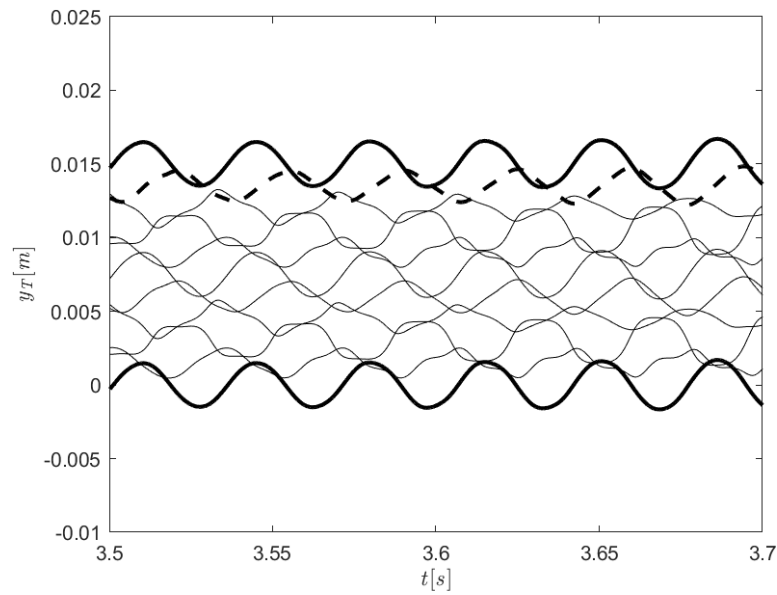


Fig. 8. Forced vertical vibration of all blades at centres of gravity at  $\Delta\varphi = -2\pi/5$

frequency 29 Hz that is almost three times higher than the excitation frequency. Other multiple maxima are caused by an amplitude modulation of the torsional resonant vibration: a) by excitation frequency in a time interval (1.8, 3) s or b) by vertical resonant vibration with frequency 92 Hz in the interval (3.7, 4) s.

#### 4.2. Study case B – Cascade with inter-blade structural connections

Aside from additional inter-blade structural connections, all initial and boundary conditions of the cascade and backward-running force excitation (Fig. 10) of the previous case were applied. The time characteristics of the first blade displacements and its aerodynamic moment show that

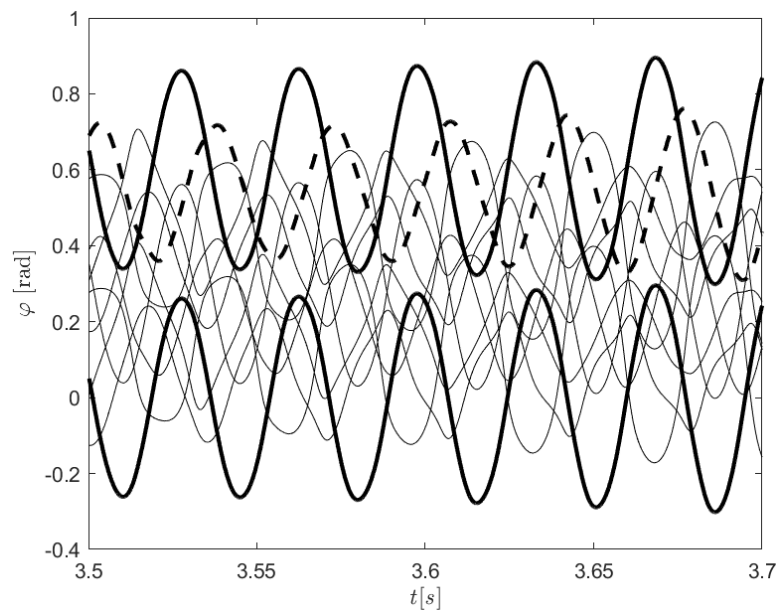


Fig. 9. Forced torsion vibration of all blades at  $\Delta\varphi = -2\pi/5$

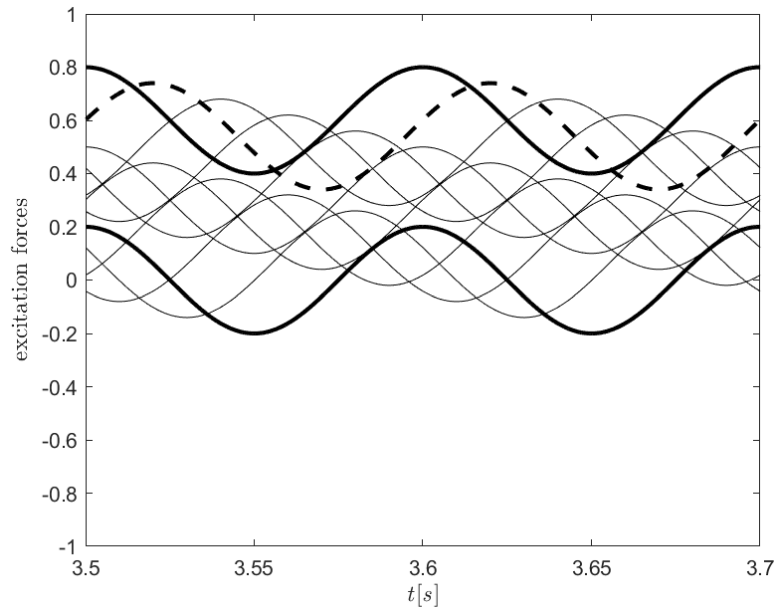


Fig. 10. Backward running force wave via cascade at  $\Delta\varphi = -2\pi/5$

the flutter arises again at time ca. 1.2 s when intensity coefficient achieves a value of  $10^{-3}$  (Fig. 14).

Due to arising self-excited vibration on the first torsional eigenfrequency, the dominant vibrations are observed at torsional mode, but it also causes an increase in vertical displacements. Vibrations reach maximum amplitude at time 1.5 s and variable amplitude-time course of vibration shows a non-stationary character.

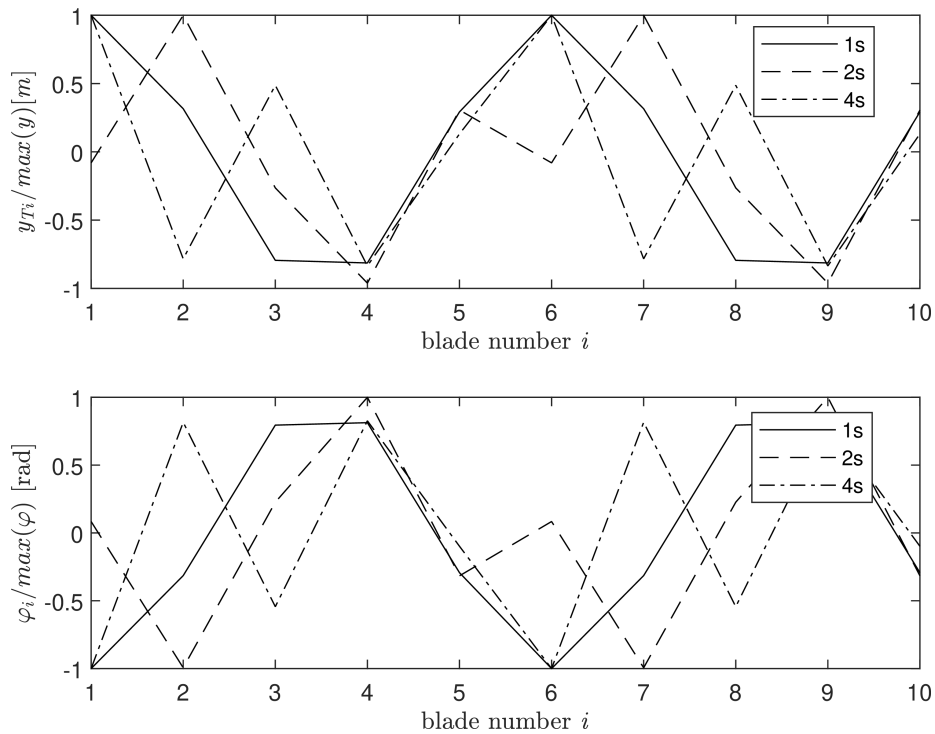


Fig. 11. Vibration modes of the cascade at the beginning (1 s) and at the flutter states (2 s and 4 s)

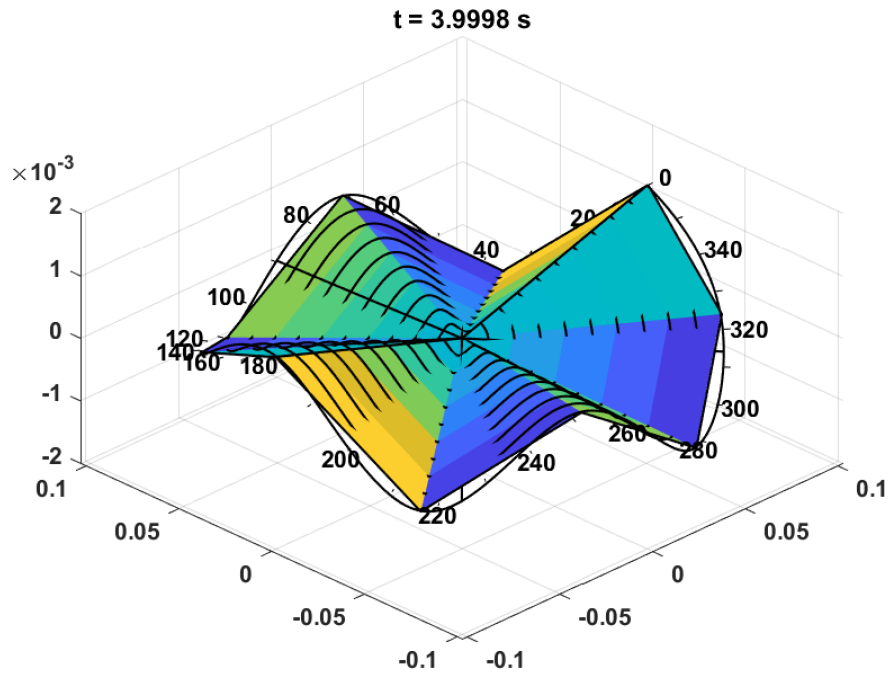


Fig. 12. The vibration mode of the wheel at time 3.999 8 s

From the phase diagrams in Fig. 15, it can be seen that the angular torsional vibration of the first blade had almost a periodical character in the first half of the loading cycle, i.e., (0, 2) s. However, it is different in the second half, i.e., (0, 4) s, when the vibration exhibits a highly

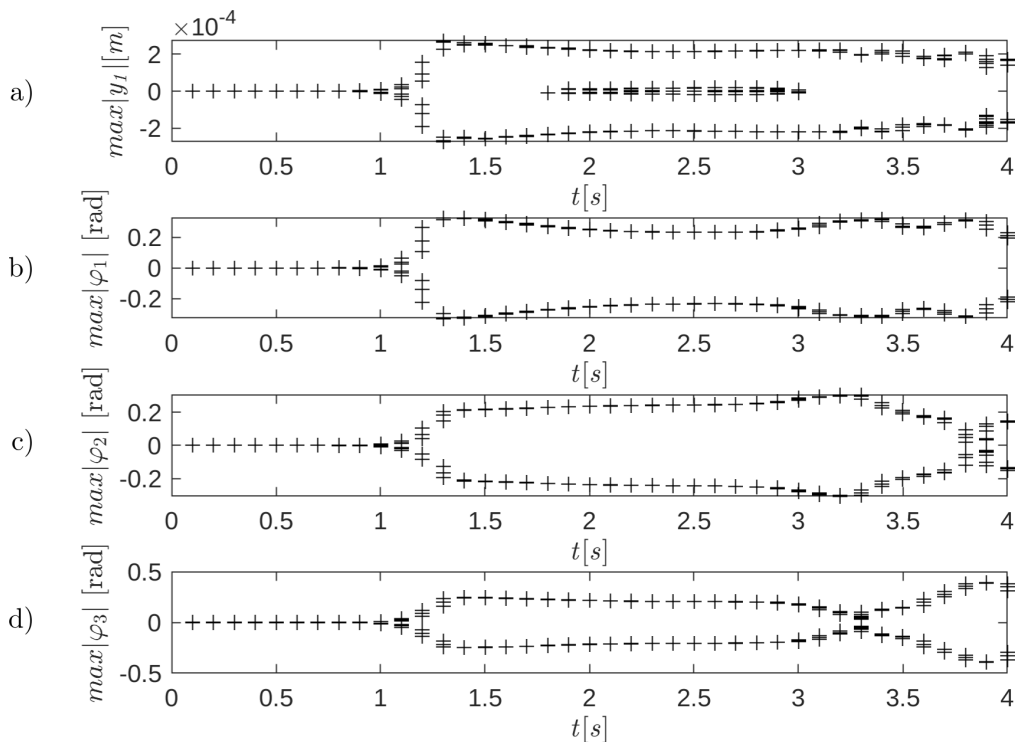


Fig. 13. Maximal amplitudes of (a) vertical and (b) angle displacement responses of the first, (c) second, (d) third blade during each period of excitation at the excitation frequency 10 Hz and  $\Delta\varphi = -2\pi/5$

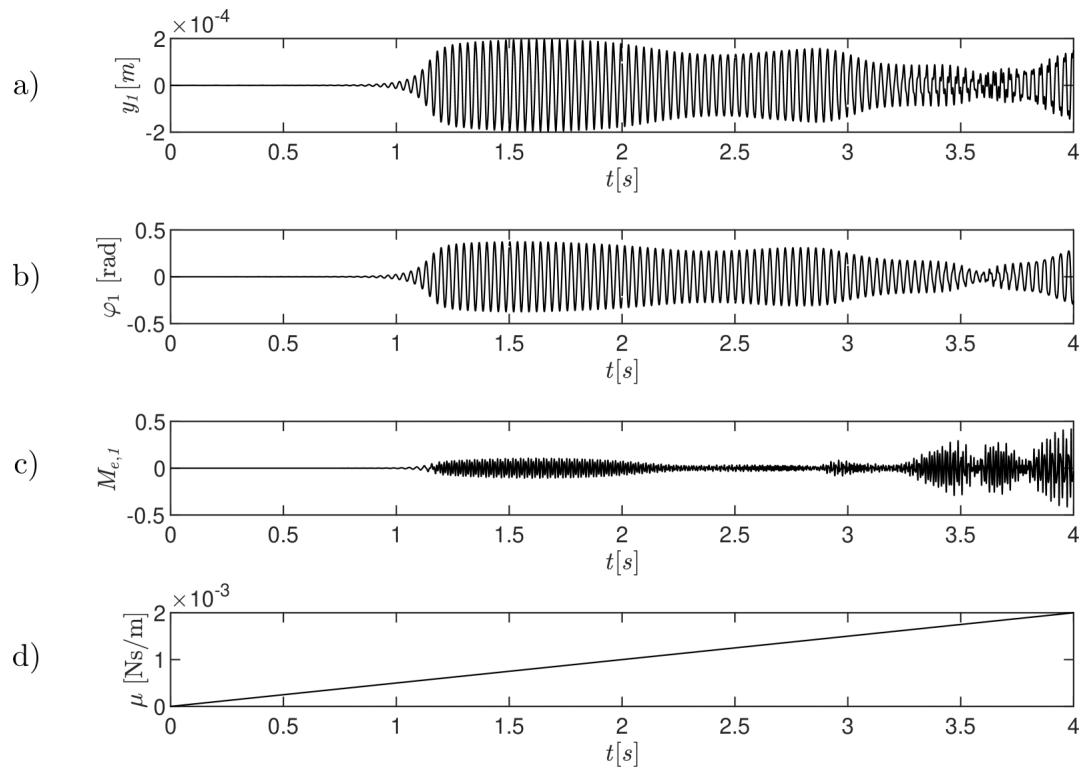


Fig. 14. Time characteristics of amplitudes of (a) vertical and (b) angular displacement responses of the first blade, of (c) aerodynamic moment of the first blade and of (d) intensity coefficient at excitation frequency 10 Hz and  $\Delta\varphi = -2\pi/5$

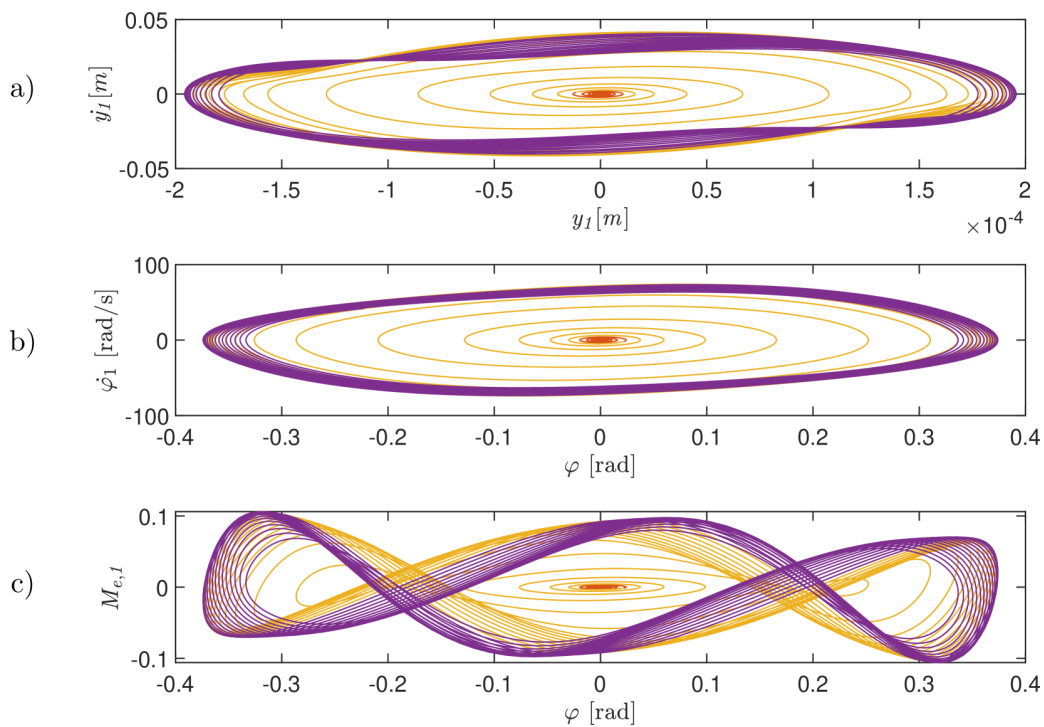


Fig. 15. Phase diagrams in interval (0, 2)s: (a) vertical and (b) angular responses of the first blade, (c) hysteresis loops of aerodynamic moment versus angle displacement of the first blade at excitation frequency 10 Hz and  $\Delta\varphi = -2\pi/5$

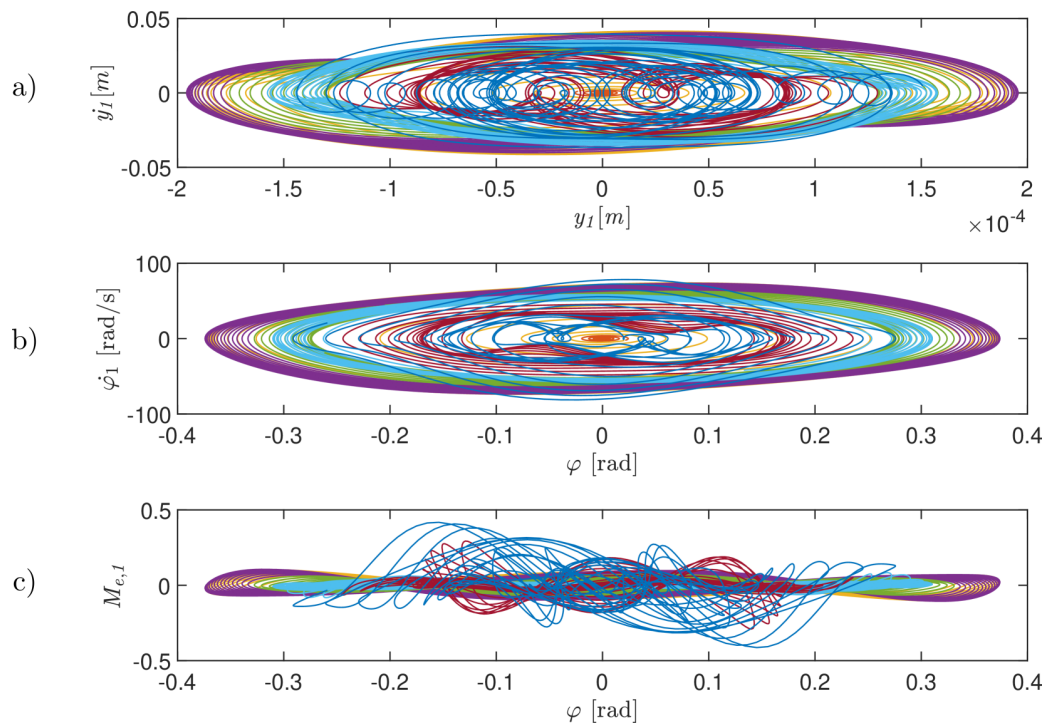


Fig. 16. Phase diagrams in interval (0, 4) s: (a) vertical and (b) angular responses of the first blade, (c) hysteresis loops of aerodynamic moment versus angle displacement of the first blade at excitation frequency 10 Hz and  $\Delta\varphi = -2\pi/5$

non-linear character for both vertical and torsional displacements (Fig. 16). The profile motion has an unstable quasi-harmonic character. The same is valid also for hysteresis curves of the aerodynamic moment. To illustrate the evolution of the phase diagram, the colours change over time with calculation intervals – red (0, 1) s, yellow (1, 1.5) s, violet (1.5, 2) s, green (2, 2.5) s, magenta (2.5, 3) s, light blue (3, 3.5) s, dark blue (3.5, 4) s.

The motions of other blades have similar time displacement and phase diagrams, but they are phase-shifted in time. The vertical and distortion displacements of all 10 blades in interval (3.5, 3.7) s are plotted in Figs. 17 and 18, respectively, and their distribution at three selected times (3.5 s, 3.75 s, 4 s) can be seen on the vibration shapes in Figs. 19 and 20, respectively.

Contrary to the study case A, the vibration in the cascade keeps the travelling character of vibraton modes even in self-excited resonant vibration state of the cascade. Both vertical transversal and torsional deformation modes are travelling with 2 ND even in a more developed state of flutter (Figs. 17–18).

In Fig. 19, we can see the mode of vibration across the cascade at longer times of the flutter state. It is clear that the mode of vibration has a dominant eigenmode shape with 2 ND. Although the backward-running force mode was applied to the cascade, due to flutter self-excitation leading to resonant vibration of the cascade, the vibration mode had a longer integration time (greater than 3.5 s) – almost the character of a standing wave, as seen in Fig. 20.

The maximal amplitude diagram (Fig. 21) shows multiple maxima during one excitation period. At the onset of self-excited oscillation (1.3 s), this phenomenon is caused by a shorter vibration period due to the resonant torsional vibration with frequency 29 Hz, which is almost three times higher than the excitation frequency. Other multiple maxima are caused by an amplitude modulation of the torsional resonant vibration: a) by excitation frequency in a time

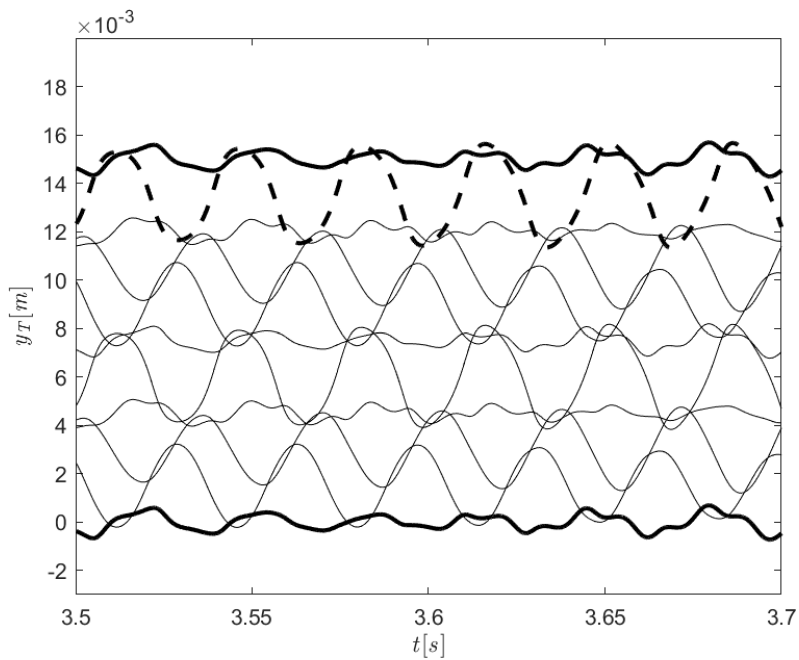


Fig. 17. Forced vertical vibration of all blades at centres of gravity at  $\Delta\varphi = -2\pi/5$

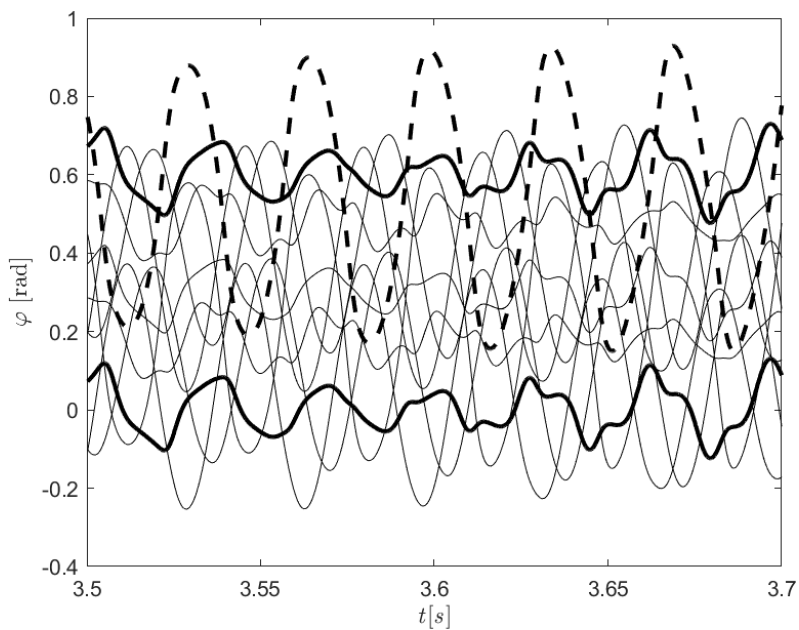


Fig. 18. Forced torsional vibration of all blades at  $\Delta\varphi = -2\pi/5$

interval (1.8, 3) s or b) by vertical resonant vibration with frequency 29 Hz in the interval (3.7, 4) s.

## 5. Conclusions

The parameters of the aeroelastic turbine wheel model were evaluated from the experiments of bladed wheels on the rotary test rig and from the aeroelastic testing of a blade cascade in the aerodynamic tunnel. The reduced model was used to describe the aeroelastic behavior of such

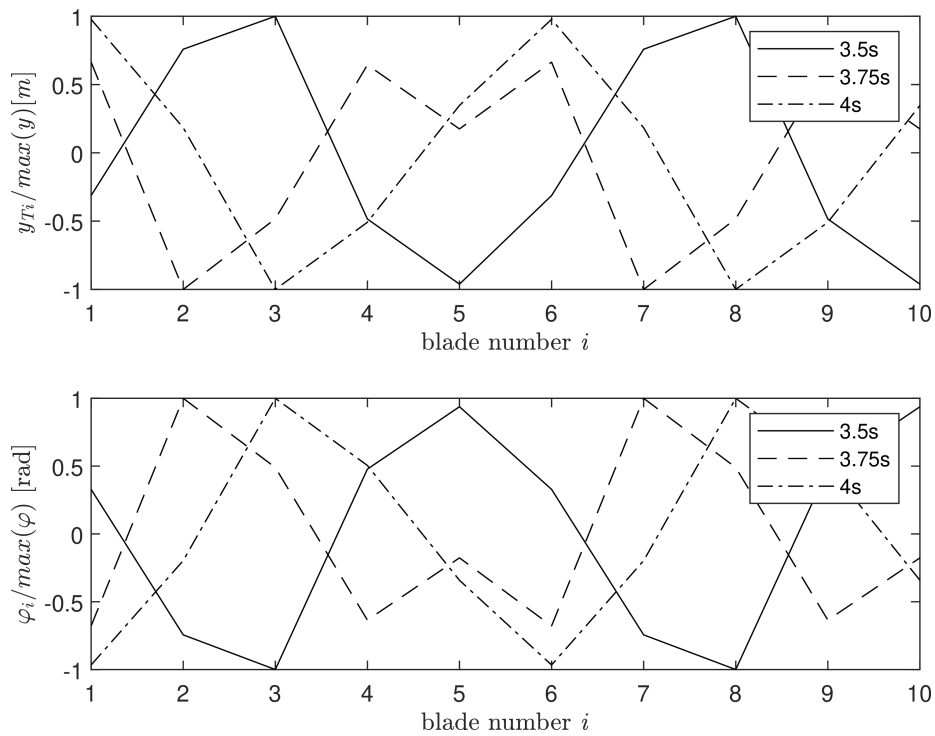


Fig. 19. Modes of vibration of the cascade at longer times of the flutter state (3.5 s, 3.75 s, 4 s) – excitation frequency 10 Hz and  $\Delta\varphi = -2\pi/5$

complex structures at the limit of stability. To model aeroelastic forces, the modified Van der Pol model controlled by relative motion of blades was considered.

The dependence of computed AD damping on the phase angle and on the number of nodal

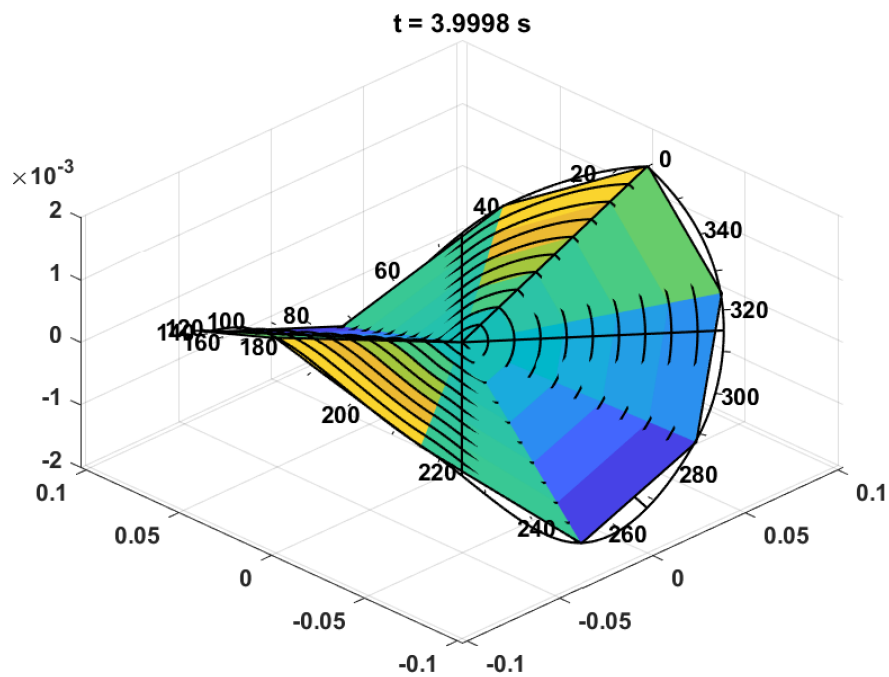


Fig. 20. Vibration mode of the wheel at 3.9998 s

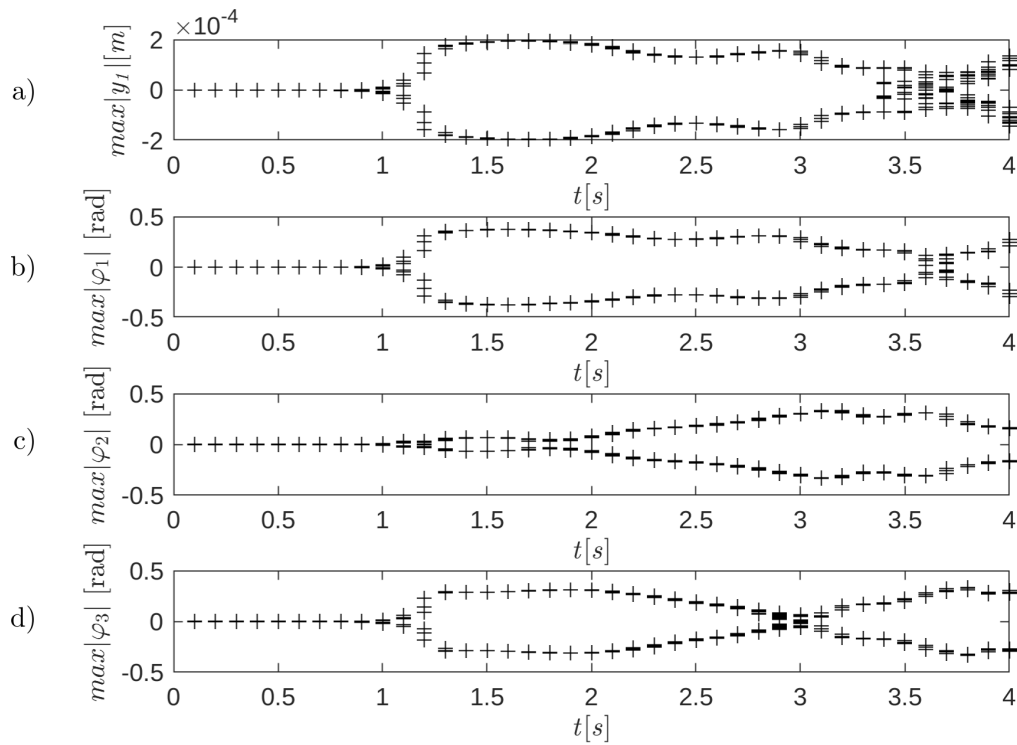


Fig. 21. Maximal amplitudes of (a) vertical and (b) angular displacement responses of the first, (c) second, (d) third blades during each period of excitation at excitation frequency 10 Hz and  $\Delta\varphi = -2\pi/5$

diameters was shown. In addition, the intensity coefficient of the flutter model can be estimated by using experimental AD damping for the travelling mode with a certain number of nodal diameters.

The flutter onset and its evolution in the cascade were simulated numerically by increasing the intensity coefficient, simulating an increase of instability in flow due to gradually increasing flow velocity. For the simulation, we chose both a study case without (A) and a case with (B) inter-blade viscoelastic Kelvin-Voigt connections. The first case corresponds to cascades without linkages between them, e.g., via disk, and only damping connections are modeled via the modified Van der Pol model of flow aeroelastic forces. In the second case, both structural and aeroelastic connections are considered.

The time characteristics of blade displacements and aerodynamic moments show that the flutter arises at time ca. 1.2 s when intensity coefficient achieves a value ca.  $10^{-3}$ . Its value is lower than the one estimated from the tuning to experimental values of AD damping. This is due to the influence of structural dynamics of the cascade that was suppressed (high structural damping of vibration) at evaluation of AD damping. In the numerical simulation of flutter vibration with increasing intensity coefficient, the dominant vibration is observed at torsional mode but it is accompanied also with an increase of vertical displacements of profiles, which is caused by arising self-excited vibrations on the first torsional eigenfrequency. Even after some stabilization of vibrations at time 1.5 s, the amplitudes of vibrations are not constant, and the course of vibration is non-stationary.

The results of both cases do not differ much at the onset and beginning of the flutter, where 2 ND travelling wave was dominant. The main differences can be seen in longer integration times, greater than 3.5 s. For the case A, a mode of 4 ND prevailed and this travelling wave became standing. In the case B, it was the vibration of the 2 ND mode that went into a standing

wave. From a practical point of view, a comparison of the two cases shows that due to the inter-blade connections, the cascade vibration mode tends to maintain the dominant shape that was originally excited due to the nozzle excitation. In the case of a cascade without inter-blade connections, the vibration mode has a higher number of nodal diameters and may have a more complex and unpredictable shape. These observations contradict the observations in our previous work [4] using the Van der Pol model controlled by total motion of individual blade, where the synchronized flutter running waves with similar properties as forced waves were numerically found. Thus, it shows that the instabilities of flutter type can make the vibration modes much more complex by inter-blade relative self-excitation, and there is a need to suppress the relative motions in the form of, e.g., inter-blade frictional damping.

The results of numerical simulations bring valuable findings about dynamic behavior of the blade cascade of turbine wheels under running nozzle excitation and arising travelling waves at the onset and development of the flutter state. The numerical simulations can be further exploited for testing a new algorithm for prediction of the flutter onset.

### **Acknowledgement**

This work was supported by the research project of the Czech Science Foundation "Study of dynamic stall flutter instabilities and their consequences in turbomachinery application by mathematical, numerical and experimental methods" [No. 20-26779S].

### **References**

- [1] Kielb, R., Barter, J., Chernycheva, O., Fransson, T., Flutter of low pressure turbine blades with cyclic symmetric modes: A preliminary design method, *Journal of Turbomachinery* 126 (2) (2004) 306–309. <https://doi.org/10.1115/1.1650380>
- [2] Pešek, L., Půst, L., Šnábl, P., Study of dry-friction damping effect on two simplified models of flutter oscillations, In: *Advances in Mechanism and Machine Science – Proceedings of the 15th IFToMM World Congress on Mechanism and Machine Science, Vol. 73*, Springer, Cham, 2019, pp. 3419–3428. Springer International Publishing. [https://doi.org/10.1007/978-3-030-20131-9\\_337](https://doi.org/10.1007/978-3-030-20131-9_337)
- [3] Prasad, C. S., Šnábl, P., Procházka, P., Chindada, S., Effect of geometrical and flow parameters on subsonic stall flutter in blade cascade, *Proceedings of IFASD 2022*, Madrid, Spain, 2022.
- [4] Půst, L., Pešek, L., Byrtus, M., Modelling of flutter running waves in turbine blades cascade, *Journal of Sound and Vibration* 436 (2018) 286–294. <https://doi.org/10.1016/j.jsv.2018.08.011>
- [5] Půst, L., Pešek, L., Interaction of self-excited and delayed forced excitation on blade bunch, *Proceedings of VETOMAC XII*, Warsaw, Poland, 2016, pp. 139–148.
- [6] Půst, L., Pešek, L., Byrtus, M., Flutter running waves in turbine blades cascade, *Proceedings of DSTA*, Lodz, Poland, 2017, pp. 483–492. <https://doi.org/10.1016/j.jsv.2018.08.011>
- [7] Půst, L., Pešek, L., Blades forced vibration under aero-elastic excitation modeled by Van der Pol, *International Journal of Bifurcation and Chaos* 27 (11) (2017) 1–12. <https://doi.org/10.1142/S0218127417501668>
- [8] Rao, J. S., *Turbomachine blade vibration*, Wiley Eastern Limited, New Delhi, 1991.
- [9] Rządowski, R., Gnesin, V., 3-D inviscid self-excited vibrations of a blade row in the last stage turbine, *Journal of Fluids and Structures* 23 (6) (2007) 858–873. <https://doi.org/10.1016/j.jfluidstructs.2006.12.003>
- [10] Schlaefli, D., *Experiments on unsteady flow effects in vibrating annular cascades*, Ph.D. thesis, École polytechnique fédérale de Lausanne (EPFL), Lausanne, 1989. (in German)

- [11] Šnábl, P., Pešek, L., Prasad, C. S., Bula, V., Cibulka, J., Experimental setup and measurement for evaluation of blade cascade stall flutter instability, In: *Advances in Acoustics, Noise and Vibration – Proceedings of the 27th International Congress on Sound and Vibration (ICSV 2021)*, Silesian University Press, Gliwice, 2021, pp. 1–5.
- [12] Vogt, D. M., Fransson, T. H., A new turbine cascade for aeromechanical testing, *Proceedings of the 16th Symposium on Measuring Techniques in Transonic and Supersonic Flow in Cascades and Turbomachines*, Whittle Laboratory, Cambridge, 2002, pp. 1–8.
- [13] Yan, L. T., Li, Q. H., Investigation of travelling wave vibration for bladed disk in turbomachinery, *Proceedings of the 3rd International Conference on Rotordynamics – IFToMM*, Lyon, France, 1990, pp. 133–135.